

Article

Separation of Molar Weight-Distributed Polyethylene Glycols by Reversed-Phase Chromatography—Analysis and Modeling Based on Isocratic Analytical-Scale Investigations

Malvina Supper ¹, Kathleen Heller ¹, Jakob Söllner ¹, Tuomo Sainio ² and Malte Kaspereit ^{1,*}

¹ Institute for Separation Science & Engineering, Friedrich-Alexander-Universität Erlangen-Nürnberg, Egerlandstr. 3, 91058 Erlangen, Germany

² School of Engineering Science, Lappeenranta-Lahti University of Technology LUT, Mikkulankatu 19, 15210 Lahti, Finland

* Correspondence: malte.kaspereit@fau.de

Abstract: The separation of polyethylene glycols (PEGs) into single homologs by reversed-phase chromatography is investigated experimentally and theoretically. The used core-shell column is shown to achieve the baseline separation of PEG homologs up to molar weights of at least 5000 g/mol. A detailed study is performed elucidating the role of the operating conditions, including the temperature, eluent composition, and degree of polymerization of the polymer. Applying Martin's rule yields a simple model for retention times that holds for a wide range of conditions. In combination with relations for column efficiency, the role of the operating conditions is discussed, and separations are predicted for analytical-scale chromatography. Finally, the approach is included in an efficient process model based on discrete convolution, which is demonstrated to predict with high accuracy also advanced operating modes with arbitrary injection profiles.

Keywords: polyethylene glycol; monodisperse PEG; reversed-phase chromatography; thermodynamic analysis; modeling



Citation: Supper, M.; Heller, K.; Söllner, J.; Sainio, T.; Kaspereit, M. Separation of Molar Weight-Distributed Polyethylene Glycols by Reversed-Phase Chromatography—Analysis and Modeling Based on Isocratic Analytical-Scale Investigations. *Processes* **2022**, *10*, 2160. <https://doi.org/10.3390/pr10112160>

Academic Editor: Alina Pyka-Pajak

Received: 30 September 2022

Accepted: 20 October 2022

Published: 22 October 2022

Publisher's Note: MDPI stays neutral with regard to jurisdictional claims in published maps and institutional affiliations.



Copyright: © 2022 by the authors. Licensee MDPI, Basel, Switzerland. This article is an open access article distributed under the terms and conditions of the Creative Commons Attribution (CC BY) license (<https://creativecommons.org/licenses/by/4.0/>).

1. Introduction

Syntheses of polymers and nanoparticles as well as the degradation of large (natural) polymers typically deliver products with a distribution of molar weight or particle size, respectively. This crucially affects product quality—the narrower its size distribution, the more valuable the product. Due to its separation power, flexibility, and scalability [1], chromatography is a promising option to narrow down the size distribution of polydisperse products. However, the small property differences within a distribution make this a challenging task, and systematic development work is required to establish efficient preparative chromatographic processes. Here, we perform corresponding investigations by analytical-scale chromatography using polyethylene glycols (PEGs) as a model system. The work should also help paving the route toward the chromatographic classification of nanoparticles [2].

The size-selective separation of PEGs is a relevant example problem. Control of the molar weight (MW) allows a precise adjustment of the PEG's specific properties. Smaller PEGs up to about PEG 800 (the number represents the weight-average MW) are intermediates for surfactants, fabric softeners and optical brighteners. Intermediate MWs such as PEG 1000 or 2000 are relevant in cosmetics [3]. These and larger MWs are particularly important in pharmaceutical applications [4], where drug molecules are PEGylated to increase their residence time in the body, facilitating more controlled and lower dosage. Here, the use of *monodisperse* PEGs (i.e., pure single homologs) instead of polydisperse PEGs is rapidly gaining importance, since it improves bio-activity and safety, allowing optimal and reproducible therapeutic results [5,6]. Monodisperse PEGs are also valuable

standards for many analytical methods, including size exclusion chromatography and various spectroscopic methods.

Monodisperse PEGs are very expensive and seem commercially available only up to MWs of about 1000 g/mol. This corresponds to a degree of polymerization (i.e., number of repetitive building blocks) of $n = 22$ (the molar weight of a PEG homolog is calculated as $(44.04 \cdot n + 18.02)$ g/mol). Some manufacturers offer larger MWs on request. However, chemical syntheses of single PEG homologs are tedious, multi-step procedures with limited yield [7]. Moreover, they deliver as side products homologs of undesired size, necessitating (chromatographic) purification. The attainable molar weight is limited. The largest homologs synthesized so far seem to be the monomethoxy-PEGs with $n = 64$ (approx. 2800 g/mol) [8].

Chromatographic separation of molar weight-distributed PEGs may be a flexible and interesting alternative, since it could provide monodisperse PEGs with intermediate MWs. For example, a simple scale-up of the methods described in this work yielded a pure single homolog of PEG 1000, which was then used for determining diffusion coefficients by heterodyne dynamic light scattering [9]. Another feature of chromatography is that it can deliver simultaneously a large number of individual homologs within a homologous series, thus including the homologs and their “direct neighbors” within a molar weight distribution (MWD). As concerns analytical chromatography, also, the accurate determination of the MWD of PEGs is of interest, in particular for medium and large MWs. Analysis of PEGs by high-performance liquid chromatography (HPLC) has been studied using reversed-phase (RP-HPLC) and normal phase (NP-HPLC) [3,10–20]. Alternatively, supercritical fluid chromatography (SFC) can be applied [21,22]. The latter was also used for a small-scale isolation of a single homolog with $n = 23$ [23]. Regarding achievable peak resolution, for example, Meyer et al. [10] achieved almost baseline resolution for PEG 2000 by RP-HPLC with a C18 column and methanol/water as eluent, and Rissler [12] demonstrated satisfactory resolution of PEG 3000 (C18 column, acetonitrile/water). NP-HPLC and RP-HPLC allow for similar performance, as shown by Sun et al. [24] for PEG 2000 (amino column, ternary solvent vs. C18 column, methanol/water). The introduction of superficially porous stationary phases allowed a further advance due to the higher number of theoretical stages of such so-called core-shell columns. For example, Xu et al. [20] demonstrated the baseline resolution of PEG 3000 using a core-shell C18 column and acetonitrile/water. A core-shell column is also studied in this work.

The separability of PEGs by RP-HPLC is dominated by three major aspects: namely, the degree of polymerization, the temperature, and the eluent composition. As regards the first, the retention of species in a homologous series can be analyzed thermodynamically using Martin’s rule [25], which states that the natural logarithm of the retention factor k' depends linearly on the degree of polymerization, n . Martin’s rule was shown to apply for many polymeric systems, including n -alkanes, n -methylesters, and n -alkylbenzenes [26], alkyl alcohols [27], polystyrenes [14,28], as well as PEGs and PEG derivatives [3,13,15–19]. The role of temperature and eluent composition in PEG separation was analyzed mainly on C18 columns in several thermodynamic studies [3,13,15], in part also for larger PEGs that could not be separated into individual homologs [13,15]. A study of column efficiency as a function of the mentioned aspects seems not yet available.

Here, we extend the existing works with the aim of establishing efficient modeling approaches for the design of analytical as well as preparative chromatographic processes. The model should be valid for the separation of PEGs in a broad range of conditions. For this purpose, we investigate the separability of PEGs of different molar weights into single homologs (up to PEG 6500) on an analytical C18 core-shell column using acetonitrile/water as eluent. A detailed study is performed for small and intermediate-sized PEGs (up to PEG 1400), in which the temperature and eluent composition are varied in rather wide ranges. From the results, an accurate retention model is derived based on Martin’s rule. Moreover, also, column efficiency is described as a function of conditions. The obtained relations are then used to evaluate the separation and to predict suitable conditions for

analytical-scale separations. Finally, an efficient model is proposed that allows the simulation of complete chromatograms also for operating concepts typical in preparative chromatography.

2. Theoretical Background

2.1. Thermodynamic Retention Model

The chromatographic separation of species is a result of the differences in their distribution equilibria between a mobile and a stationary phase, respectively. The distribution equilibrium of a component between two phases holds the fundamental relation

$$\Delta G^\circ = \Delta H^\circ - T\Delta S^\circ = -RT \ln K. \quad (1)$$

In Equation (1), ΔG° , ΔH° , and ΔS° are the standard free energy, standard enthalpy, and standard entropy, respectively, while T is temperature. The distribution coefficient, K , can be related to the chromatographic retention factor under linear conditions, k' , by

$$k' = \frac{t_R - t_0}{t_0} = FK, \quad (2)$$

with t_R as the retention time of the component, and t_0 as the residence time in the column's void volumes. F is the phase ratio, i.e., the volumetric ratio of stationary and mobile phase. From Equations (1) and (2) follows

$$\ln k' = -\frac{\Delta H^\circ}{RT} + \frac{\Delta S^\circ}{R} + \ln F. \quad (3)$$

If the phase ratio F is independent of temperature and solvent composition, its contribution can be included into an apparent entropy change, ΔS^* . Equation (3) then reads

$$\ln k' = -\frac{\Delta H^\circ}{RT} + \frac{\Delta S^*}{R}. \quad (4)$$

Since F is typically below unity, ΔS^* is a reasonable approximation for ΔS° [13] (potential deviations from this are discussed in [29]). Based on measuring the retention times of a component at different temperatures, $t_R(T)$, Equation (4) allows determining ΔH and ΔS^* from a van't Hoff plot, i.e., as the slope and ordinate intercept of $\ln k'$ plotted against $1/T$.

As concerns molar weight-distributed polymers, the retention of molecules in a homologous series is often described well by Martin's rule [25]. The latter states that the free energy of a molecule corresponds to the sum of the contributions of its molecular building units. Thus, for a macromolecule, ΔG° is a linear function of its degree of polymerization n . Consequently, Equation (4) can be written for each species of a homologous series as

$$\ln k'_n = -\frac{\Delta H_n^\circ}{RT} + \frac{\Delta S_n^*}{R}, \quad (5)$$

where the enthalpic and entropic contributions are linear functions of n ,

$$\Delta H_n^\circ = n \Delta H_r^\circ + \Delta H_e^\circ, \quad (6a)$$

$$\Delta S_n^* = n \Delta S_r^* + \Delta S_e^*. \quad (6b)$$

The subscripts r and e in Equations (6) denote the repeat units and the end groups of the polymer, respectively. Thus, if determined values of ΔH_n° and ΔS_n^* are found to depend linearly on n , one can determine the individual contributions ΔH_r° , ΔH_e° , ΔS_r^* , and ΔS_e^* by linear regression. More details on Martin's rule can be found in the literature. A discussion in the classical context of partition chromatography (Martin's original scope) is given

in [30], while its fundamentals and thermodynamic interpretation in interaction-based chromatography are addressed in, for example [31,32].

Separability can be assessed by a separation factor α between two consecutive homologs of size n and $(n + 1)$ defined as the ratio of their retention factors, i.e., $\alpha = k'_{n+1}/k'_n$. In conjunction with Equations (5) and (6), one obtains

$$\ln \alpha = \ln \left(\frac{k'_{n+1}}{k'_n} \right) = -\frac{\Delta H_r^\circ}{RT} + \frac{\Delta S_r^*}{R}. \quad (7)$$

Equation (7) shows that if Martin's rule applies, for a given set of conditions (e.g., constant temperature and eluent composition in an isocratic chromatographic experiment), the separation factor between any pair of neighbors in a homologous series depends only on the contribution of a single repetitive unit, ΔH_r° and ΔS_r^* , while it is independent of the size of the molecules (degree of polymerization, n) and of their end groups, respectively.

Values for k' allow describing only the distance between peaks, but not the extent of their separation, since the latter depends also on band broadening. The actual separation can be quantified by the peak resolution, R ,

$$R = 2 \frac{t_{R,n+1} - t_{R,n}}{w_{n+1} + w_n} \approx 1.18 \frac{t_{R,n+1} - t_{R,n}}{w_{1/2,n+1} + w_{1/2,n}}, \quad (8)$$

where w and $w_{1/2}$ denote the width and width at half-height, respectively, of the corresponding peak. So-called baseline separation is achieved for about $R > 1.5$.

In Section 4.2, the above relations are applied to evaluate an extensive experimental study of RP-HPLC of PEGs, and to determine parameters for a thermodynamic model describing the separation in a broad range of molar weight, temperature, and mobile phase composition.

2.2. Column Model Based on Discrete Convolution

A number of powerful models exists that are capable of predicting complete chromatograms [33]. However, for the problem at hand—a large number of mixture components and very high stage numbers—their accurate numerical solution becomes very slow.

Discrete convolution is a simple and efficient approach for predicting the output of linear, time-invariant systems. It requires only the applied input signal and the system's impulse response. Chromatography behaves as a linear transfer system provided the involved distribution equilibria are linear and no nonlinear mass transfer effects occur. This usually holds for size exclusion chromatography (SEC) as well as for analytical chromatography, where concentrations are low. Convolution models were used, for example, for designing the SEC-based purification of human influenza virus [34] and integrated processes that combine SEC and reactive hydrolysis to produce oligo- from polysaccharides [35].

Below, we summarize the approach for modeling linear chromatography. The concentration of a component i at the column outlet, $c_{out,i}(t)$, is obtained by convolution of its injection time profile, $c_{inj,i}(t)$, with the residence time distribution (RTD) of the component, $E_i(t)$,

$$c_{out,i}(t) = c_{inj,i}(t) * E_i(t), \quad i = (1, N). \quad (9)$$

The asterisk (*) in Equation (9) denotes the convolution operation, which is defined as

$$c_{out,i}(t) = \int_0^t c_{inj,i}(t - t') E_i(t') dt'. \quad (10)$$

Equation (10) can be solved in the Laplace domain, where convolution corresponds simply to multiplying the Laplace transforms of the input profile and the residence time distribution, i.e.,

$$c_{out,i}(t) = \mathcal{L}^{-1} \{ \mathcal{L} [c_{inj,i}(t)] \mathcal{L} [E_i(t)] \}. \quad (11)$$

In some cases (e.g., Dirac pulse injections and suitable RTDs, see also below), Equation (11) can be solved analytically. This allowed establishing many fundamental relations in the frame of plate theory of chromatography, in particular for the analysis of mass transfer and dispersion; see e.g., [1]. More details on using Laplace transformation for modeling linear chromatographic processes are given in [36,37].

In many cases, however, the analytical back-transformation in Equation (11) is not possible, e.g., if arbitrary injection profiles $c_{inj,i}(t)$ must be considered, or if the RTD function $E_i(t)$ accounts for complex mass transfer effects. In such cases, discrete convolution can be performed numerically after the time-discretization of Equation (10). A well-known illustrative example is given in Levenspiel's textbook [38]. It is even easier to apply fast Fourier transform, as already suggested by Villiermaux [36,39]. Solving Equation (11) then simply corresponds to

$$c_{out,i}(t) = \text{IFFT} \{ \text{FFT}[c_{inj,i}(t)] \cdot \text{FFT}[E_i(t)] \}, \quad (12)$$

where FFT and IFFT denote here corresponding commands for fast Fourier transform and its inverse, respectively, as available in standard calculus software. This approach is computationally very fast, which makes it particularly suitable for multi-component systems as considered here.

For simulating chromatograms for the PEG system studied, we apply the well-known RTD function,

$$E_i(t) = \frac{1}{\sigma_i \sqrt{2\pi}} \exp \left[-\frac{1}{2} \left(\frac{t - \mu_i}{\sigma_i} \right)^2 \right]. \quad (13)$$

Equation (13) is the solution of the classical tanks-in-series model by Martin and Synge [40] for a Dirac-pulse injection onto an efficient column (i.e., stage number larger than about 100), see e.g., [1,41]. It is a normal distribution with μ_i as the first absolute moment of the pulse response for component i . For symmetrical peaks, this equals the retention time, $\mu_i = t_{R,i}$. The values for μ_i will be obtained here from the retention model described in Section 2.1. The second parameter in Equation (13) is the standard deviation of the peak, σ_i , which is related to the number of theoretical stages, NTP_i , by [1]

$$NTP_i = \frac{\mu_i^2}{\sigma_i^2}. \quad (14)$$

The values of both, μ_i and σ_i , are obtained easily from chromatograms for small injections as performed in this study.

3. Experimental

3.1. Materials

Commercial PEG standards with narrow MWDs served as chromatographic samples. Specifically, we used PEG 200 (average molar weight specified by manufacturer: 222 g/mol), 400 (434 g/mol), 600 (626 g/mol), 1400 (1400 g/mol), 3000 (n/a), 4200 (4240 g/mol), and 6500 (6550 g/mol), respectively. Except for PEG 3000 (Sigma-Aldrich, Taufkirchen, Germany), all standards were purchased from Phenomenex (Aschaffenburg, Germany).

Chromatographic eluents were prepared using HPLC gradient grade acetonitrile (VWR, Darmstadt, Germany) and ultrapure water from a purification unit (Aquinity2, membraPure, Hennigsdorf, Germany).

3.2. Chromatographic Separation

The chromatographic experiments were performed using a liquid chromatography/mass spectrometry (LC/MS) setup. The used Ultimate 3000 LC unit (Dionex, Sunnyvale/CA, USA) consisted of a gradient pump LPG-3400A with degasser, a column thermostat TCC-3000, and an autosampler WPS-3000SL. Detection was performed by a charged aerosol detector (CAD; Corona Ultra RS, Thermo Fisher Scientific, Dreieich, Germany). The eluting

PEG homologs were identified based on their molar weights using the MS (ABI SciexQTrap, Sciex, Darmstadt, Germany), which analyzed a small side stream delivered by a splitter. Details on the MS analysis are given in the Supplement (*ibid.*, Section S1). For data acquisition, the software Chromeleon 6.80 (Dionex) and Analyst (Sciex) were used.

All chromatograms were obtained in isocratic mode using a Kinetex C18 core-shell column (100×4.6 mm, particle diameter $2.6 \mu\text{m}$, pore size 100 \AA ; Phenomenex) connected to a precolumn with the same packing (2×4.6 mm). Acetonitrile/water mixtures served as eluent at a flow rate of 1 mL/min . Injected samples were $10 \mu\text{L}$ of 1 g/L total PEG in ultrapure water.

The experiments were performed at five different temperatures ($15, 20, 30, 40,$ and 50°C) and at nine different mobile phase compositions ($15, 17, 19, 21, 22, 23, 24, 25,$ and 27.5 vol\% acetonitrile in water). The binary eluents were premixed to the desired ratios based on gravimetric measurements. The column was equilibrated before injection for 20 min if the eluent composition was altered and for 40 min if the temperature was changed. After each experiment, the complete elution of all remaining components was ensured in a 5 min blank run with a forced elution step (acetonitrile concentration increased to 50 vol\% for 1 min).

4. Results and Discussion

4.1. Separation Problem and Role of Operating Conditions

Figure 1 shows example chromatograms that illustrate the separation problem and the interplay between the molar weight of the homologs and the chromatographic operating conditions in terms of temperature and eluent composition.

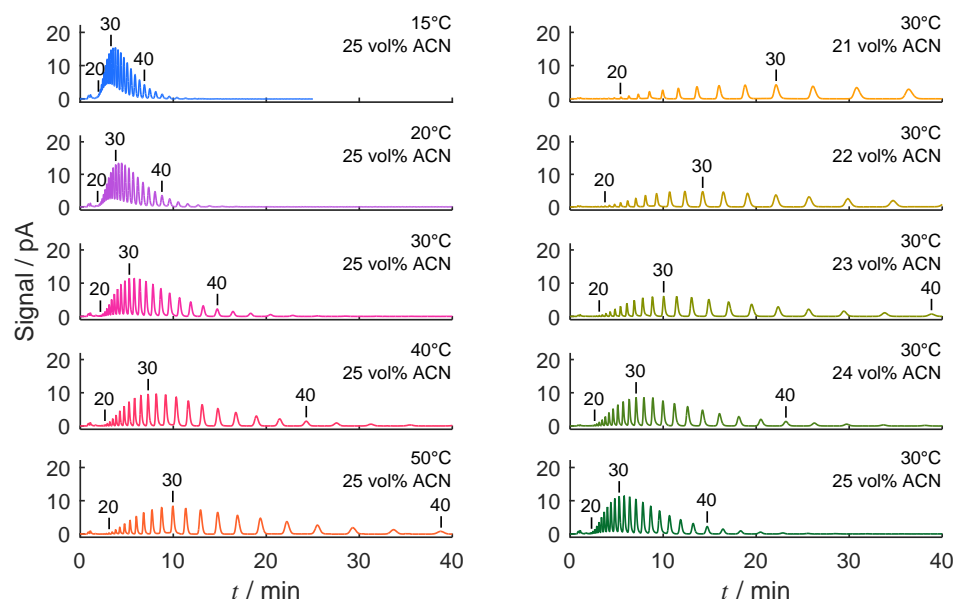


Figure 1. Example chromatograms demonstrating the roles of temperature and mobile phase composition for the separation of PEG 1400. For better orientation, peaks are marked for the homologs with $n = 20, 30,$ and $40,$ respectively. **Left**—five different temperatures ($15, 20, 30, 40, 50^\circ\text{C}$), using 25 vol\% acetonitrile (ACN) in water as eluent. **Right**—five different eluent compositions ($21, 22, 23, 24,$ and 25 vol\% ACN in water) at 30°C . Remark: The chromatogram in the left (middle) is the same as the one in the right (bottom).

First, one observes that the used PEG standards contain—despite their narrow MWDs—a significant number of homologs. In the case of PEG 1400 shown in Figure 1, 32 homologs were quantified within the detection limits with degrees of polymerization ranging from $n = 15$ to 46 . The determined MWD, which can be described by a Gaussian normal distribution, is shown in Figure 2. The polydispersity of this sample was calculated as $M_w/M_n = 1.02$, which is within the manufacturer's specification of $M_w/M_n \leq 1.05$.

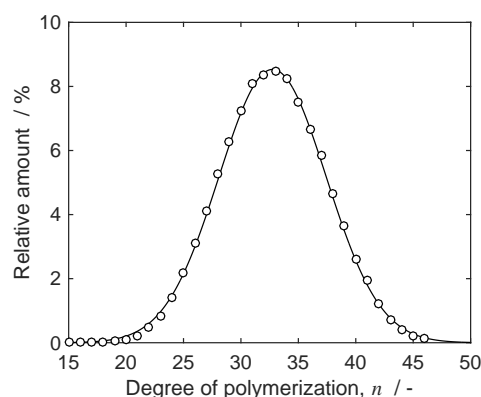


Figure 2. Molar weight distribution of PEG 1400 determined chromatographically (symbols) and interpolation by Gaussian normal distribution (line; mean value 32.754, standard deviation 4.676). Measured at 44 °C and 25 vol % ACN in water.

The inspection of Figure 1 reveals that retention increases strongly with the increasing degree of polymerization, n . This is expected from the exponential nature of Martin's rule (see Section 2.1) and will be studied in detail in Section 4.2.

The role of temperature, T , is demonstrated by the chromatograms in Figure 1 (left) obtained at five different temperatures between 15 and 50 °C for a constant eluent composition (25 vol % acetonitrile, ACN, in water). Obviously, retention of the homologs increases with T . While at 15 °C (Figure 1, top left), all homologs elute between 2 and 12 min; at 50 °C (bottom left), the retention times of the largest homologs are beyond 40 min. This dependency on T is unusual. In most cases, adsorption on surfaces is exothermic, i.e., $\Delta H_i^\circ < 0$ in Equation (4), in which case k'_i decreases with T . The opposite behavior seen here is known for PEGs for some reversed-phase systems, e.g., [13,15,18]. The sign of ΔH_i° depends on the nature of the eluent. $\Delta H_i^\circ > 0$ was found for PEGs on C18 columns when using ACN/water [13,15,18] or acetone/water [18] as eluent, while $\Delta H_i^\circ < 0$ was observed for methanol/water [18] as well as in normal-phase chromatography [15]. Cho et al. [15] attributed the peculiar retention of PEGs on C18 for ACN/water eluents to hydrophobic interactions. Interaction of the amphiphilic PEGs with the stationary phase causes a release of water molecules and, thus, a net entropy increase larger than the enthalpic contribution. With increasing T , the latter decreases relative to the entropy effect, which causes increasing retention. This interpretation is also supported by partitioning experiments by Spitzer et al. [42] and could explain why the solubility of PEGs in water decreases with temperature.

In addition, the chromatograms indicate that not only retention but also peak resolution increases with T . At 15 °C (Figure 1, top left), the peaks are separated only partially. At 30 °C (middle left), peaks of homologs with $n_i \geq 30$ are baseline separated, and at 50 °C (bottom left), all significant peaks are separated completely. This can be explained by the temperature dependencies of both thermodynamic parameters and mass transfer resistances, as discussed in Sections 4.3 and 4.4.

Figure 1 (right) demonstrates the influence of mobile phase composition. PEG retention decreases markedly with increasing ACN level. For example, when increasing ACN from 21 to 25 vol %, the retention time of the homolog $n = 30$ decreases from 22 min to only 5 min; that for $n = 40$ decreases even from about 2 h (beyond axis limit) to less than 15 min, respectively. The role of ACN as a desorption-promoting agent [15] was observed in various studies (e.g., [13,15,18]). It results from the dependencies of the entropic and enthalpic interactions on the ACN level, as discussed in Section 4.2. Finally, it is emphasized that experimentally, the pronounced sensitivity of retention toward the ACN level has to be carefully accounted for.

To demonstrate the separation power of RP-HPLC in connection with using core-shell columns, Figure 3 shows example chromatograms for larger PEGs. Conditions were chosen such to obtain a baseline resolution ($R \geq 1.5$). For PEG 3000 (Figure 3, top), a relatively

constant resolution of $R \approx 2.2$ is achieved for all homologs $n = 53$ (retention time 6 min) through $n = 90$ (110 min). In case of PEG 4200 (Figure 3, middle), R drops slightly from 2.0 for $n = 70$ (45 min) to 1.5 for $n = 96$ (380 min). PEG 6500 (Figure 3, bottom) contains many homologs with $n < 80$ that elute at low retention times (see inset of Figure 3, bottom). For $n \approx 80$ (22 min) up to about $n = 113$ (160 min), the baseline is straight, and R is between 1.5 and 1.6. Beyond 160 min, the valley-to-valley integration of peaks still gives $R \approx 1.5$, but the rising 'baseline' indicates probably increasing overlaps of neighboring peaks. Note that the MW of the last homolog shown, $n = 129$ (410 min), is with 5700 g/mol still below the mean MW of PEG 6500. It should be mentioned that samples with larger MW required larger injection amounts to obtain clear signals (see labels in Figure 3). This is due to the higher temperatures used (alternatively, the ACN level might be lowered) for their separation. This leads to (impractically) long run times and, thus, strong dilution. Furthermore, the higher a sample's mean MW, the more homologs are present in its MWD in correspondingly lower amounts.

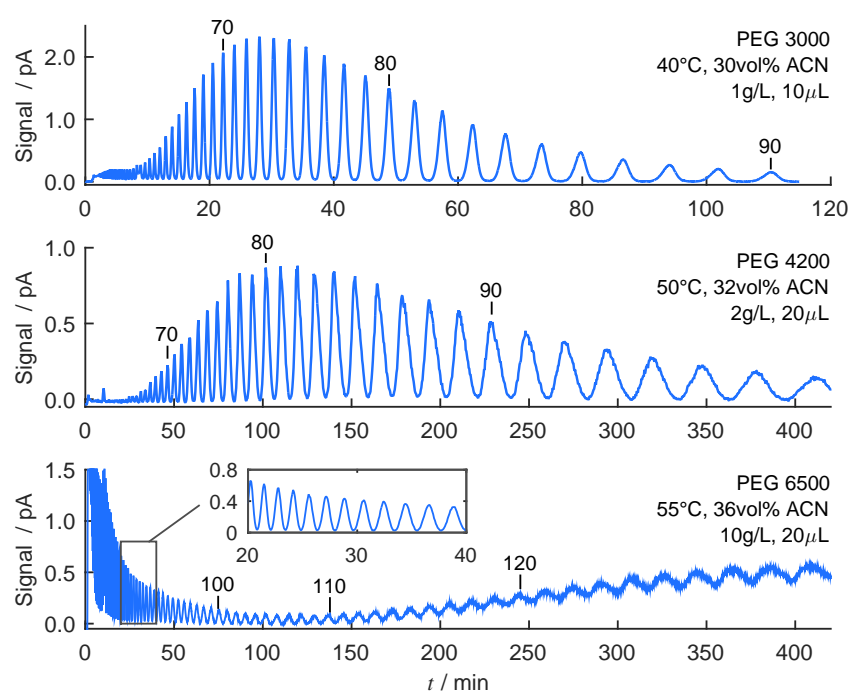


Figure 3. Selected examples for the separation of larger PEGs. Conditions (see labels) were adjusted to achieve about baseline resolution. **Top**—PEG 3000 (average degree of polymerization $\bar{n} = 68$). **Middle**—PEG 4200 ($\bar{n} = 95$; the actual average MW was estimated as 3900 g/mol). **Bottom**—PEG 6500 ($\bar{n} = 136$). The inset shows the separation of the many small homologs with low retention times.

Overall, the achievable separation is remarkable when considering that for the shown examples, the difference in molar weight between two neighboring homologs is about 1% and less. Baseline resolution was achieved for PEG homologs up to at least $n = 113$, corresponding to an MW of about 5000 g/mol. To our knowledge, such resolution by RP-HPLC has not yet been demonstrated.

4.2. Thermodynamic Parameters

In the following, we determine the parameters for the thermodynamic retention model in Equations (5) and (6) as well as for the process model, as shown in Equations (12) and (13), respectively. For this, chromatograms were measured in the temperature range between 15 and 50 °C, and acetonitrile (ACN) contents were measured between 15 and 27.5 vol%. Depending on the separability at the given conditions, PEG standards of different molar weight (PEG 200, 400, 600, and 1400) were used. Due to the excessively long run times required for sufficient resolution, larger PEGs as in Figure 3 were not analyzed.

Measurements were performed in triplicate, and only peaks with a minimum resolution of $R \geq 1.4$ were evaluated.

For the evaluation, k'_i values for each homolog need to be calculated from the measured peak retention times. The latter are corrected by the residence time in the column's external system volume, t_{sys} . Thus, Equation (2) is rewritten as

$$k'_n = \frac{t_{R,n} - t_{sys} - t_0}{t_0}, \quad (15)$$

where $t_{R,n}$ is the measured retention time of the corresponding homolog. Note that when using Equations (5) and (6) for parameter determination, the correction by t_{sys} influences the value of ΔS_e^* only. ΔH_r° , ΔH_e° , and ΔS_r^* are not affected, and they could be determined using Equation (2) without knowledge of t_{sys} . We determined $t_{sys} = 0.247$ min from a small injection of uracil bypassing the column with a zero-volume connector. Furthermore, a value for t_0 is required, which should correspond to the residence time of solutes in the column's accessible volume. Wang et al. [19] as well as Trathnigg [17,18] underlined that erroneous results may be obtained when determining t_0 by pycnometry or from the retention times of tracer peaks. According to their works, the appropriate way to determine t_0 is to evaluate the retention time *differences* between neighbors in a homologous series. From Equations (7) and (15) follows for two neighboring homologs n and $n + 1$

$$t_{R,n} = \frac{t_{R,n+1} - t_{R,n}}{\alpha - 1} + t_0 + t_{sys}. \quad (16)$$

As pointed out in Section 2.1, the separation factor $\alpha = k'_{n+1}/k'_n$ in Equation (16) is independent of n if Martin's rule applies. In this case, a plot of $t_{R,n}$ vs. $(t_{R,n+1} - t_{R,n})$ will yield a straight line with the sum $(t_0 + t_{sys})$ as ordinate intercept.

Figure 4 (left) exemplifies this for the five chromatograms in Figure 1 (left). All data follow straight lines with almost identical ordinate intercepts. The same holds true for the other conditions examined, confirming the applicability of Trathnigg's [16–18] approach. Averaged over all evaluated chromatograms, $(t_0 + t_{sys}) = 0.988 \pm 0.05$ min was determined. With the above value of t_{sys} , we obtain $t_0 = 0.741$ min, which corresponds to a phase ratio of $F = 1.24$. In the studied parameter range, t_0 was found to be practically independent of temperature and mobile phase composition. However, Wang et al. [19] showed that the accessible volume is constant only up to about 30 vol % ACN, and it increases beyond this value. We could confirm this in initial tests for larger PEGs that require high levels of ACN for separation (data not included here). Models for larger PEGs and high ACN concentrations will have to consider this.

Next, the retention factors k' are determined from Equation (15) for all measured chromatograms. As an example, Figure 4 (right) shows the results for the chromatograms in Figure 1 (left). The $\ln k'$ values for all series follow straight lines, confirming the validity of Martin's rule. Linear plots were also obtained for all other conditions. It is worth mentioning that when t_0 values calculated from pycnometry or tracer peaks were used, the obtained Martin's plots were not linear.

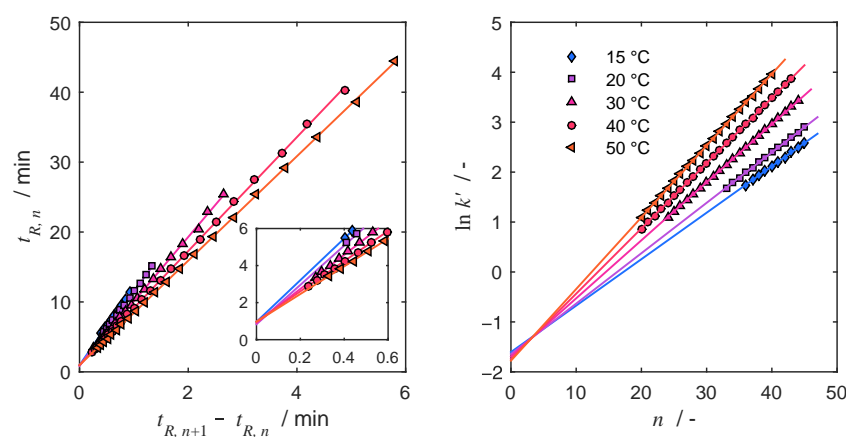


Figure 4. Evaluation of chromatograms exemplified for the temperature series for PEG 1400 in Figure 1 (left) at 25 vol % ACN. **Left**—Determination of t_0 along Trathnigg's method from the axis intercept in Equation (16). **Right**—Martin's plot for the same data, underlining the linear dependency of $\ln k'$ on n .

With the applicability of Martin's rule confirmed, the thermodynamic parameters of the retention model can be determined. As shown in Figure 5 (left), a van't Hoff plot ($\ln k'$ vs. $1/T$) of the data from Figure 1 (left) yields almost perfectly straight lines. According to Equation (5), the linear regression for each homolog n delivers ΔH_n^0 and ΔS_n^* as the slopes and intercepts, respectively. In Figure 5, these values are plotted against n , which gives, again, linear trends. The slopes and intercepts of these lines are the enthalpic and entropic contributions in Equation (6) for the repetitive units (ΔH_r^0 , ΔS_r^*), and the end groups (ΔH_e^0 , ΔS_e^*), respectively. This procedure was performed for all mobile phase compositions, and in all cases, linear van't Hoff plots and linear dependencies on n were obtained. The corresponding diagrams are given in the supplement (*ibid.*, Figures S3–S6).

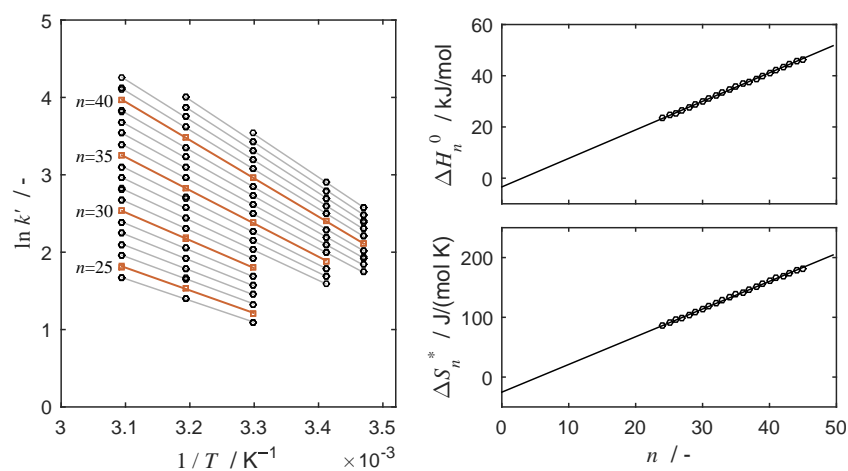


Figure 5. Determination of thermodynamic parameters for PEG 1400 at the same conditions as in Figure 1 (left) (25 vol % acetonitrile). **Left**—van't Hoff plot of data (symbols, triplicate measurements) and linear regression against Equation (5) (lines) for the different homologs. **Right**—enthalpic and entropic contributions as a function of n corresponding to the slopes (ΔH_n^0) and intercepts (ΔS_n^*) of the lines in the left (symbols). Linear regression against Equation (6) (lines) delivers ΔH_r^0 , ΔH_e^0 and ΔS_r^* , ΔS_e^* as slopes and intercepts, respectively.

Table 1 lists the determined parameters as a function of the ACN content. Most relevant are the enthalpic and entropic contributions of the repetitive units, ΔH_r^0 and ΔS_r^* , since they are dominating for the molar weights studied here. Both values are larger than zero, and their average values of about 1 kJ/mol and 5 J/mol/K, respectively, compare quite well to literature data (see the last three lines in Table 1). ΔH_r^0 and ΔS_r^* increase with

increasing ACN, which both contribute to decreasing retention. Overall, when evaluating the terms $-\Delta H_n^\circ/RT$ and $\Delta S_n^*/R$ for different conditions, one finds that the entropy term affects retention slightly stronger than the enthalpic term. The impact of the latter increases with ACN, decreasing T , and decreasing n . For the smallest homologs, the enthalpic contribution can become slightly dominating (e.g., for $n = 15$ at 15°C and 27.5 vol % ACN).

Table 1. Determined thermodynamic parameters as function of the acetonitrile content (ACN) of the mobile phase and comparison to literature data.

Sample	ACN vol%	ΔH_r° kJ/mol	ΔH_e° kJ/mol	ΔS_r^* J/(mol K)	ΔS_e^* J/(mol K)
PEG 1400 (this work)	15.0	0.715	−2.465	4.861	−24.285
	17.0	0.929	−3.241	5.171	−26.520
	19.0	0.994	−3.076	5.027	−25.629
	21.0	1.083	−3.509	5.006	−26.432
	22.0	1.090	−3.245	4.893	−25.299
	23.0	1.077	−2.992	4.742	−24.434
	24.0	1.094	−3.320	4.684	−24.950
	25.0	1.114	−3.410	4.639	−25.263
	27.5	1.132	−4.771	4.481	−29.251
PEG 600 [18]	11.1	1.1 ^a	−2.8 ^a	5.9 ^a	−13.0 ^a
PEG 2300 [15]	35.0	1.23	14.0 ^b	4.39	30.0 ^b
	45.0	0.52	-	1.68	-

^a Estimated from Figure 9 (ΔH°) and Figure 10 (ΔS^*) in [18]. ^b Estimated from Figure 3 in [15].

While we observe a slight increase of ΔH_r° with the increasing ACN level, it remains open if this trend will continue for larger ACN concentrations. For a somewhat larger PEG and higher ACN levels (35 and 45 vol %), Cho et al. [15] observed a decrease of ΔH_r° (last two lines in Table 1).

Finally, a fully explicit retention model for calculating k' as function of n , T , and ACN level from Equations (5) and (6) is obtained by interpolating ΔH_r° , ΔH_e° , ΔS_r^* , and ΔS_e^* in Table 1 as a function of ACN. Figure 6 shows that a good fit is obtained when using third-order polynomials (for parameters, see Table 2).

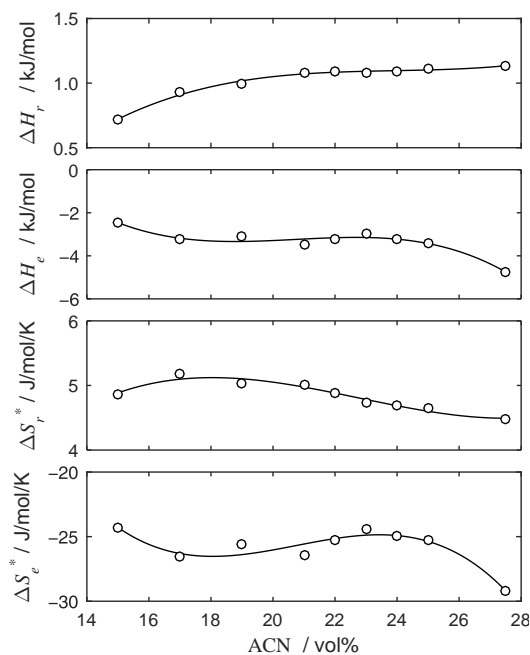


Figure 6. Thermodynamic parameters as function of the mobile phase composition. Symbols—parameters determined from measured retention times (see text). Lines—Interpolation by third-order polynomials.

It is worth mentioning that retention factors and thermodynamic parameters as determined above are helpful for developing a better understanding of RP-HPLC of macromolecules. They can serve, for example, as reference values for corresponding Monte Carlo simulations [43,44].

Table 2. Polynomial coefficients for interpolation of the thermodynamic parameters in Table 1 as function of the acetonitrile content. Calculation in the form $y = \sum_i p_i \cdot x^i$ with $y = (\Delta H_r^\circ, \Delta H_e^\circ, \Delta S_r^*, \Delta S_e^*)$ and x as ACN content in vol%. Enthalpies in kJ/mol and entropies in J/(mol K).

	p_3	p_2	p_1	p_0
ΔH_r°	0.000472	−0.033848	0.814105	−5.467108
ΔH_e°	−0.006433	0.399831	−8.210674	52.4509195
ΔS_r^*	0.001490	−0.101743	2.216156	−10.494034
ΔS_e^*	−0.021576	1.342734	−27.387407	157.230293

4.3. Column Efficiency

From the measured chromatograms, also column efficiency in terms of NTP can be assessed. The corresponding values were determined automatically for all individual homologs in all chromatograms by the data acquisition software, using the well-known approximation of Equation (14),

$$NTP_i = 5.54 \frac{t_{R,i}^2}{w_{1/2,i}^2}, \quad (17)$$

where $t_{R,i}$ and $w_{1/2,i}$ are the retention time and the width at half height of the peak of homolog i , respectively.

In contrast to the evaluation of retention times, which yielded ‘clean’ linear trends in the frame of the theory, the NTP values deliver a more complex picture. Figure 7 exemplifies this for the chromatograms obtained using PEG 1400. Again, only peaks with a resolution of $R \geq 1.4$ were considered. First, one recognizes that the rather short core-shell column is remarkably efficient, showing NTP values up to about 15,000. Second, one observes that NTP generally increases with the degree of polymerization, n . The reason for this is the strongly increasing sorption with n , which reduces the dispersion due to mass transfer resistances. This effect is stronger than the increasing dispersion due to slower free bulk diffusion for larger n . Third, NTP decreases with increasing ACN level (see Figure 7, left), while it increases with T (Figure 7, right). Obviously, also here, the strongly increasing sorption is responsible for the effects of both T and ACN on NTP .

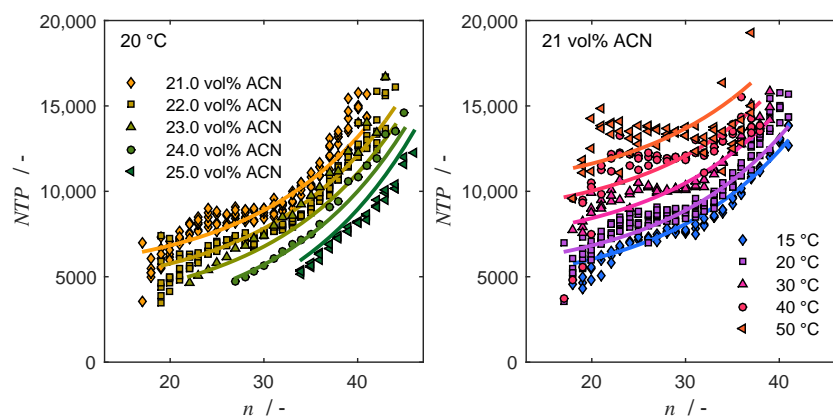


Figure 7. Dependence of NTP on polymerization degree, temperature, and acetonitrile content for PEG 1400. **Left**— NTP values of the individual homologs at 20 °C for different ACN levels. **Right**— NTP values at 21 vol % ACN for different temperatures. Evaluated were all chromatograms for PEG 1400; multiple values for the homologs due to repetitive measurements.

Apart from these general trends, one notices fluctuations of the determined *NTP* values for the same homologs. We attribute this to the fact that the determination of the half-height widths in Equation (17) becomes very sensitive in particular for small homologs, whose peaks are very narrow.

Another observation is that the course of *NTP* over *n* is somewhat uneven and may even have local minima. This indicates that the determined values are biased. A close inspection of Figure 1 reveals that peaks for lower *n* are slightly asymmetric, which indicates nonlinear sorption. Consequently, it is likely that displacement effects occur between the homologs due to competitive sorption. This sharpens peaks and thereby increases the determined *NTP*, in particular for the smaller *n* that elute earlier and closer together. At the same time, for homologs in the middle of an MWD, the determined *NTP* may be too low, since their concentration is much higher than that of smaller or larger ones. Thus, the uneven course of *NTP* and the apparent minima can be explained by the interplay of the decreasing mass transfer effects with increasing *n*, increased peak sharpening for small homologs, and the different concentrations of the homologs within the MWD. This hypothesis is strengthened when analyzing chromatograms of PEGs with different average MWs, where the same homologs elute as early or late ones and at different concentrations. Obtaining a clear picture on the ‘true’ *NTP* values will require injecting different pure homologs at identical concentration. These are not available commercially. Producing them by preparative chromatography is under investigation but beyond the scope of this work.

Despite the above, it is emphasized that the thermodynamic model from Section 4.2 predicts retention times accurately. Moreover, combining this with a model for the (biased) *NTP* data will allow for a precise prediction also of resolution in the investigated range of conditions—at least for samples with a similar MWD as those used for the parameterization of *NTP*. Here, we apply a simple interpolation function that includes the dependencies of *NTP* on *n*, *T*, and ACN,

$$NTP(n, T, ACN) = q_1 + q_2 T + q_3 ACN + q_4 \exp(q_5 n). \quad (18)$$

Fitting Equation (18) to the data from all PEG 1400 injections (not only those shown in Figure 7) delivers a reasonable approximation of *NTP* (solid lines in the same figure). Obtained parameter values (q_i) are given in Table 3. Note that the interpolation is empirical and must be used with care. The parameters given lead to negative *NTP* values for high ACN levels, low temperatures, and low *n*.

Table 3. Parameters of Equation (18) for the interpolation of *NTP* values.

$q_1/-$	q_2/K^{-1}	$q_3/vol\%^{-1}$	$q_4/-$	$q_5/-$
−19,664.2	159.82	−1059.81	436.453	0.07349

4.4. Evaluation and Prediction of Separation under Analytical Conditions

The models for retention and column efficiency established in the previous sections are applied here for evaluating the impact of the operating conditions on the separation.

Equation (7) shows that the separation factor between neighboring homologs, $\alpha_{(n+1)/n}$, depends on the enthalpic and entropic contributions of only the repetitive groups, ΔH_r° and ΔS_r^* —but not on the degree of polymerization, *n*. The latter is confirmed in all our chromatograms, where we find a constant selectivity $\alpha_{(n+1)/n}$ between neighboring homologs. However, it should be mentioned that some studies for smaller PEGs reported an increase of selectivity with increasing *n* in the low MW range [31].

The role of temperature can be assessed from the derivative of Equation (7) with respect to *T*,

$$\frac{d \ln \alpha_{(n+1)/n}}{dT} = \frac{\Delta H_r^\circ}{RT^2}. \quad (19)$$

Since for our data, ΔH_r° is always positive (see Table 1), it follows from Equation (19) that also $d \ln \alpha_{(n+1)/n} / dT$ is always positive. Accordingly, for the studied PEG system, not only retention but also the separation factor increases with T , which confirms the observations from the chromatograms in Figure 1.

The role of acetonitrile can be evaluated similarly. For this, the polynomials for ΔH_r° , ΔH_e° , ΔS_r^* , and ΔS_e^* given in Table 2 are substituted into Equation (7). Since the derivative of Equation (7), $d \ln \alpha_{(n+1)/n} / dACN$, is found negative for the determined parameters, the separation factor increases here with decreasing acetonitrile level at least in the considered range of conditions. This is also confirmed when inspecting the chromatograms in Figure 1 (right).

The thermodynamic model allows accurate prediction of retention times (examples will be given in Section 4.5). In analytical chromatography, the resolution R (defined in Equation (8)) between peaks is of particular interest. R can be expressed for two neighboring ‘Gaussian’ peaks as a function of k' , α , and NTP by the following expression (for alternative formulae, see [45]),

$$R = \sqrt{NTP_{n+1} NTP_n} \frac{\alpha_{(n+1)/n} - 1}{\alpha_{(n+1)/n} + 1} \frac{\bar{k}'}{(1 + k'_n) \sqrt{NTP_{n+1}} + (1 + k'_{n+1}) \sqrt{NTP_n}}, \quad (20)$$

where \bar{k}' is the averaged value between both homologs.

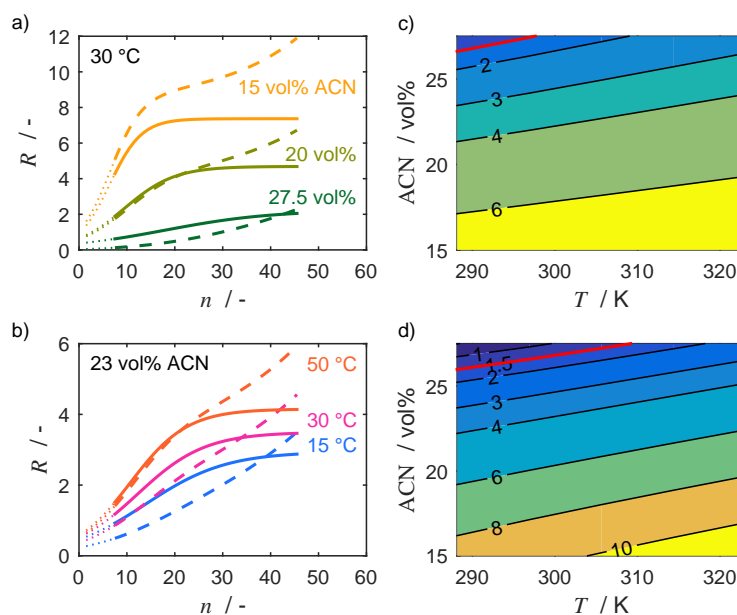


Figure 8. Prediction of peak resolution R . **Left**—Resolution R versus degree of polymerization n for different conditions: **(a)** role of mobile phase composition for constant T , **(b)** role of T at constant mobile phase composition. Solid lines— R calculated using average stage number of $\overline{NTP} = 9700$, dashed— R calculated using NTP interpolation, dotted—extrapolation for small homologs not covered by the model parametrization. **Right**—Contour maps of resolution achievable between the homologs $n = 32$ and $n = 33$: **(c)** Calculated using average $\overline{NTP} = 9700$, **(d)** using NTP interpolation. The red lines mark conditions where baseline resolution ($R=1.5$) is achieved.

Figure 8 shows the results of evaluating Equation (20) for different scenarios. As can be seen in Figure 8a,b, resolution increases with the increasing size of the homologs. Furthermore, for systems with constant NTP (solid lines), R reaches a plateau for larger n . If thermodynamics of retention (k' and α) are fixed due to the chemical nature of the involved phases, further improvement of R can be achieved only by increasing NTP . This underlines the usefulness of high-efficiency columns to resolve larger homologs. In comparison, using the interpolated NTP (dashed lines), which should give a higher degree

of accuracy, significant deviations can be observed. Specifically, R increases further also for larger n , which is due to NTP increasing with n (see Section 4.3). Detailed models will have to account for this.

Finally, it is also possible to use Equation (20) for predicting suitable operating conditions for homologs of given size. This is demonstrated by the contour maps in Figure 8 (right) for the example of homologs $n = 32$ and $n = 33$. The maps allow selecting the temperature and acetonitrile content that are required to achieve a certain desired value of resolution. Again, differences arise when assuming constant NTP , Figure 8c, or interpolated NTP values, as shown in Figure 8d. However, conditions required for baseline separation ($R = 1.5$, red lines) are similar. It is worth noting that such contour maps may give helpful indications also for designing gradients of solvent strength or temperature.

4.5. Prediction of Chromatograms Based on Convolution Model

The approach in the previous section is particularly suited for analytical chromatography, for example, to predict suitable temperatures and ACN levels to achieve sufficient resolution of PEGs of a given molar weight.

In contrast, for the design of preparative chromatography, the simulation of complete chromatograms is of interest. For very small (Dirac) injections, this is possible explicitly by solving Equation (13) for each single homolog. However, the typically larger injections in preparative chromatography have more or less 'distorted' rectangular profiles. Moreover, in operating policies such as closed-loop recycling (CLR) [46,47] or steady-state recycling (SSR) [48–50], the profiles of repetitive injections represent partially resolved chromatograms. In addition, pre-column injection mixers as used sometimes in polymer chromatography [51] will affect the injection profiles. The discrete convolution approach in Section 2.2 allows considering such arbitrary injection profiles.

First, we validate the model against an independent experiment measured at conditions not considered in the determination of the thermodynamic parameters. For this, the small injection (10 μL) is described as a rectangular pulse of corresponding length, with the injected concentrations of the homologs taken from the normal distribution of the MWD in Figure 2. The first moments, μ_i , in the RTD, Equation (13), are calculated from the k'_i values predicted by the thermodynamic model in Section 4.2. The standard deviations, σ_i , follow either from averaged NTP values or from the interpolation by Equation (18). The experimental detector signal is converted to concentration by a calibration constant calculated from the injected and the total area of the chromatogram.

As shown in Figure 9 (top), the model achieves a very good prediction of the experiment. The slight deviations for smaller homologs (see insets) are due to the nonlinear effects discussed earlier. When using the more detailed interpolation for NTP (Equation (18); dashed line) instead of an averaged value of $\overline{NTP} = 9700$ for all homologs (solid line), the agreement improves further.

Since the injection in the previous example is close to a Dirac pulse, we include also a more complex case where two columns (I and II) of the same type are connected in series, and a larger injection (100 μL) is performed. For modeling, the convolution is performed consecutively for both columns. For column I , again, a rectangular injection and the same RTD as above is used (only t_0 needed to be re-determined, since a different pre-column was required). The input for column II is then the calculated output of column I . Since the RTD of column II differs slightly, it was determined from a small injection at the same conditions, and retention was described in the form of Martin's rule as $\ln k'_i = An + B$, with A and B as fitted parameters. Due to the high pressure drop, the experiment was conducted at a lower flow rate of 0.7 mL/min, for which the NTP model above does not hold. For the sake of simplicity, we used for both columns an average value of $\overline{NTP} = 10,000$ for each homolog, which corresponds to the average in the measured chromatogram.

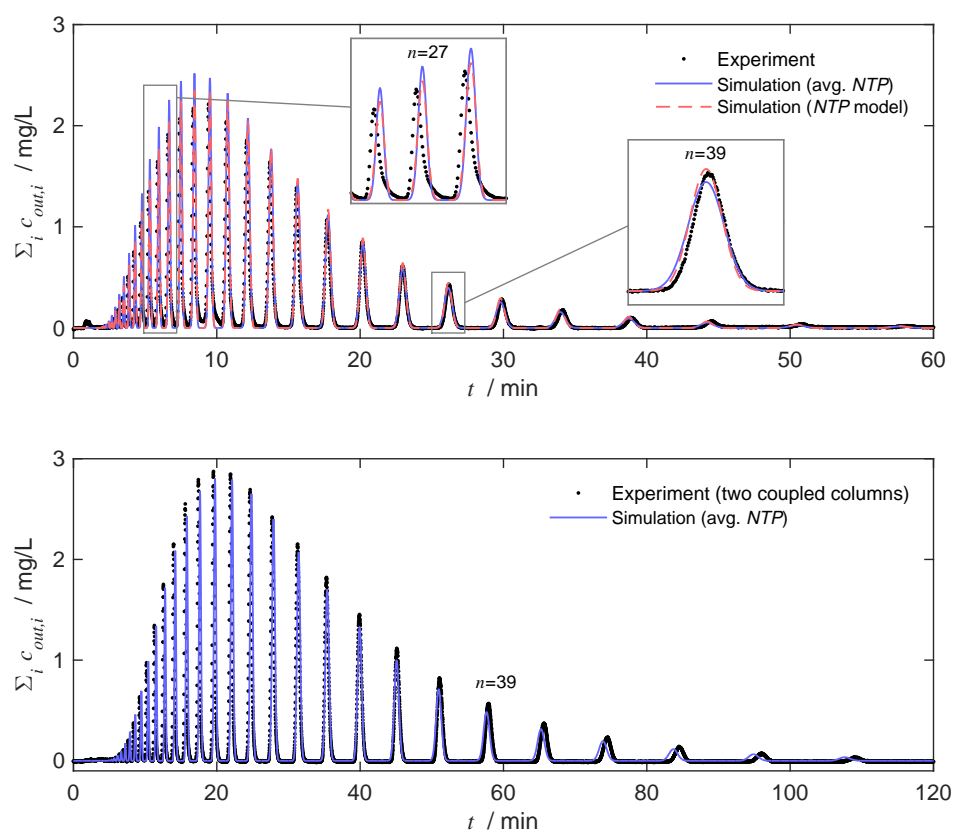


Figure 9. Validation of the modeling approach by discrete convolution. Symbols—experimental data, lines—simulated total outlet concentration, $\Sigma_i c_{out,i}(t)$, acc. to Equation (12). **Top**—Independent experiment not used for parameter determination (25 vol % ACN, 43.8 °C, 1 mL/min, 10 μ L of PEG 1400, 1 g/L). Simulations with averaged ($\overline{NTP} = 9700$) and interpolated values for NTP , respectively. **Bottom**—Experiment with two coupled columns of the same size, simulated with averaged $\overline{NTP} = 10,000$ for each column (25 vol % ACN, 40 °C, 0.7 mL/min, 100 μ L of PEG 1400, 0.1 g/L).

The simulation and experiment for the coupled column scenario are compared in Figure 9 (bottom). As expected, the combined columns achieve a much higher resolution of the homologs. More importantly, the agreement between the model and experiment is very good also in this more complex situation.

The results above underline that the proposed modeling approach—the use of a sound thermodynamic retention model in conjunction with discrete convolution—provides an efficient tool for accurate predictions of conventional and advanced chromatographic processes.

5. Summary

A systematic study has been performed for the separation of PEGs into single homologs by reversed-phase HPLC using a core-shell column. The baseline resolution of PEGs with a polymerization degree of at least 113 (5000 g/mol) was demonstrated.

Using molar weight-distributed standards of smaller and medium-sized PEGs up to 1400 g/mol, a detailed analysis of retention as a function of temperature, mobile phase composition, and molar weight was carried out. The applicability of Martin's rule was confirmed. The latter was then used to establish an accurate thermodynamic model for the retention as a function of the mentioned conditions. The determined data may be valuable also for theoretical studies of chromatographic retention.

Column efficiencies obtained from the same experiments were remarkably high. The number of theoretical stages, NTP , was found to increase with the size of the homologs, increasing temperature, and decreasing acetonitrile levels. A closer analysis revealed that in particular, incompletely resolved chromatograms deliver biased NTP values, which is most probably due to competitive sorption.

Combining the retention model with an interpolation of *NTP* values facilitated the prediction of temperatures and mobile phase compositions required to achieve a desired resolution of homologs of given size. It was demonstrated that resolution is indeed affected by the mentioned biased efficiency data, but that reasonable predictions are possible also when using averaged *NTP* values.

Finally, the retention model was included into an approach for simulating chromatograms based on discrete convolution. High accuracy was achieved when predicting chromatograms obtained from single columns as well as when emulating preparative recycling processes by connecting two columns in series.

The approach presented in this work is considered useful not only for analytical chromatography but also for the conceptual design of preparative processes that aim at producing narrow or monodisperse fractions from polydisperse polymers or nanoparticles.

Supplementary Materials: The following supporting information can be downloaded at: <https://www.mdpi.com/article/10.3390/pr10112160/s1>, S1. Detection and identification of the PEG homologs; Table S1: Parameter settings for the mass spectrometer and the charged aerosol detector; Figure S1: CAD chromatogram and the corresponding total ion count over time for PEG1400 at 23 vol % ACN and 30 °C. The injection volume was 10 µL, injected concentration 1 g/L, and flow rate 1 mL/min, respectively; S2. Thermodynamic parameters; Figure S2: Three mass spectrograms for three selected peaks at 10, 19 and 34 min derived from the chromatogram of the total ion count (Figure S1). Possible load carriers as well as double (2+) and triple (3+) charged ion sources are marked. The corresponding peaks of the three homologs ($n = 30, 35$ and 39) are marked in the CAD and MS chromatograms of Figure S1; Figure S3: Determination of thermodynamic parameters at 15 vol % (top) and 17 vol % (bottom) ACN; Figure S4: Determination of thermodynamic parameters at 19 vol % (top) and 21 vol % (bottom) ACN; Figure S5: Determination of thermodynamic parameters at 22 vol % (top) and 23 vol % (bottom) ACN; Figure S6: Determination of thermodynamic parameters at 24 vol % (top) and 27.5 vol % (bottom) ACN.

Author Contributions: Conceptualization, M.K. and T.S.; methodology, all authors; experimental investigation, M.S., K.H. and J.S.; writing—original draft preparation, M.S. and M.K.; writing—review and editing, all authors; visualization, M.K. and M.S.; supervision, M.K.; project administration, M.K.; funding acquisition, M.K. All authors have read and agreed to the published version of the manuscript.

Funding: This work was funded by the Deutsche Forschungsgemeinschaft (DFG, German Research Foundation)—Project-ID 416229255-SFB 1411.

Data Availability Statement: Not applicable.

Acknowledgments: The authors are grateful to Benedikt Bornschein, Moritz Moß, and Anna Brünner who performed some of the experiments, and to Jannis Beutel for his valuable support regarding the mass spectrometer.

Conflicts of Interest: The authors declare no conflict of interest.

References

1. Guiochon, G.; Shirazi, D.G.; Felinger, A.; Katti, A.M. *Fundamentals of Preparative and Nonlinear Chromatography*, 2nd ed.; Academic Press: Boston, MA, USA, 2006.
2. Süß, S.; Michaud, V.; Amsharov, K.; Akhmetov, V.; Kaspereit, M.; Damm, C.; Peukert, W. Quantitative Evaluation of Fullerene Separation by Liquid Chromatography. *J. Phys. Chem. C* **2019**, *123*, 16747–16756. [[CrossRef](#)]
3. Trathnigg, B.; Veronik, M. A thermodynamic study of retention of poly(ethylene glycol)s in liquid adsorption chromatography on reversed phases. *J. Chromatogr. A* **2005**, *1091*, 110–117. [[CrossRef](#)] [[PubMed](#)]
4. Wu, T.; Chen, K.; He, S.; Liu, X.; Zheng, X.; Jiang, Z.X. Drug Development through Modification of Small Molecular Drugs with Monodisperse Poly(ethylene glycol)s. *Org. Process Res. Dev.* **2020**, *24*, 1364–1372. [[CrossRef](#)]
5. Vicent, M.J.; Dieudonné, L.; Carbajo, R.J.; Pineda-Lucena, A. Polymer conjugates as therapeutics: Future trends, challenges and opportunities. *Expert Opin. Drug Deliv.* **2008**, *5*, 593–614. [[CrossRef](#)] [[PubMed](#)]
6. Yu, Z.; Bo, S.; Wang, H.; Li, Y.; Yang, Z.; Huang, Y.; Jiang, Z.X. Application of Monodisperse PEGs in Pharmaceuticals: Monodisperse Polidocanols. *Mol. Pharm.* **2017**, *14*, 3473–3479. [[CrossRef](#)] [[PubMed](#)]
7. Bohn, P.; Meier, M.A.R. Uniform poly(ethylene glycol): A comparative study. *Polym. J.* **2020**, *52*, 165–178. [[CrossRef](#)]

8. Zhang, H.; Li, X.; Shi, Q.; Li, Y.; Xia, G.; Chen, L.; Yang, Z.; Jiang, Z.X. Highly Efficient Synthesis of Monodisperse Poly(ethylene glycols) and Derivatives through Macrocyclization of Oligo(ethylene glycols). *Angew. Chem. Int. Ed.* **2015**, *54*, 3763–3767. [[CrossRef](#)]
9. Wu, W.; Supper, M.; Rausch, M.H.; Kaspereit, M.; Fröba, A.P. Mutual Diffusivities of Binary Mixtures of Water and Poly(ethylene) Glycol from Heterodyne Dynamic Light Scattering. *Int. J. Thermophys.* **2022**, *43*, 177. [[CrossRef](#)]
10. Meyer, T.; Harms, D.; Gmehling, J. Analysis of polyethylene glycols with respect to their oligomer distribution by high-performance liquid chromatography. *J. Chromatogr. A* **1993**, *645*, 135–139. [[CrossRef](#)]
11. Rissler, K. High-performance liquid chromatography and detection of polyethers and their mono(carboxy)alkyl and -arylalkyl substituted derivatives. *J. Chromatogr. A* **1996**, *742*, 1–54. [[CrossRef](#)]
12. Rissler, K. Improved separation of polyethylene glycols widely differing in molecular weight range by reversed-phase high performance liquid chromatography and evaporative light scattering detection. *Chromatographia* **1999**, *49*, 615–620. [[CrossRef](#)]
13. Lochmüller, C.; Moebus, M.A.; Liu, Q.; Jiang, C.; Elomaa, M. Temperature Effect on Retention and Separation of Poly(ethylene glycols) in Reversed-Phase Liquid Chromatography. *J. Chromatogr. Sci.* **1996**, *34*, 69–76. [[CrossRef](#)]
14. Chang, T.; Lee, H.C.; Lee, W.; Park, S.; Ko, C. Polymer characterization by temperature gradient interaction chromatography. *Macromol. Chem. Phys.* **1999**, *200*, 2188–2204. [[CrossRef](#)]
15. Cho, D.; Park, S.; Hong, J.; Chang, T. Retention mechanism of poly(ethylene oxide) in reversed-phase and normal-phase liquid chromatography. *J. Chromatogr. A* **2003**, *986*, 191–198. [[CrossRef](#)]
16. Trathnigg, B.; Skvortsov, A. Determination of the accessible volume and the interaction parameter in the adsorption mode of liquid chromatography. *J. Chromatogr. A* **2006**, *1127*, 117–125. [[CrossRef](#)] [[PubMed](#)]
17. Trathnigg, B.; Jamelnik, O. Characterization of different reversed phase systems in liquid adsorption chromatography of polymer homologous series. *J. Chromatogr. A* **2007**, *1146*, 78–84. [[CrossRef](#)]
18. Nguyen Viet, C.; Trathnigg, B. Determination of thermodynamic parameters in reversed phase chromatography for polyethylene glycols and their methyl ethers in different mobile phases. *J. Sep. Sci.* **2010**, *33*, 464–474. [[CrossRef](#)]
19. Wang, M.; Mallette, J.; Parcher, J.F. Comparison of void volume, mobile phase volume and accessible volume determined from retention data for oligomers in reversed-phase liquid chromatographic systems. *J. Chromatogr. A* **2011**, *1218*, 2995–3001. [[CrossRef](#)]
20. Xu, L.; Shahid, S.; Shen, J.; Emanuelsson, E.A.C.; Patterson, D.A. A wide range and high resolution one-filtration molecular weight cut-off method for aqueous based nanofiltration and ultrafiltration membranes. *J. Membr. Sci.* **2017**, *525*, 304–311. [[CrossRef](#)]
21. Shimada, K.; Sato, K.; Lusenkova, M.A.; Kinugasa, S.; Kudo, K.; Yamauchi, Y. Separation of Oligomers by Supercritical Fluid Chromatography. *Kobunshi Ronbunshu* **2001**, *58*, 541–547. [[CrossRef](#)]
22. Takahashi, K.; Kinugasa, S.; Senda, M.; Kimizuka, K.; Fukushima, K.; Matsumoto, T.; Shibata, Y.; Christensen, J. Quantitative comparison of a corona-charged aerosol detector and an evaporative light-scattering detector for the analysis of a synthetic polymer by supercritical fluid chromatography. *J. Chromatogr. A* **2008**, *1193*, 151–155. [[CrossRef](#)] [[PubMed](#)]
23. Takahashi, K. Advanced reference materials for the characterization of molecular size and weight. *J. Phys. Mater.* **2020**, *1193*, 146–150. [[CrossRef](#)]
24. Sun, C.; Baird, M.; Simpson, J. Determination of poly(ethylene glycol)s by both normal-phase and reversed-phase modes of high-performance liquid chromatography. *J. Chromatogr. A* **1998**, *800*, 231–238. [[CrossRef](#)]
25. Martin, A.J.P. Some Theoretical Aspects of Partition Chromatography. *Symp. Biochem. Soc.* **1949**, *3*, 4–20.
26. Colin, H.; Krstulović, A.M.; Gonnord, M.F.; Guiochon, G.; Yun, Z.; Jandera, P. Investigation of selectivity in reversed-phase liquid chromatography-effects of stationary and mobile phases on retention of homologous series. *Chromatographia* **1983**, *17*, 9–15. [[CrossRef](#)]
27. Yanagihara, Y.; Yasukawa, K.; Tamura, U.; Uchida, T.; Noguchi, K. Characteristics of a new HPLC column packed with octadecyl-bonded polymer gel. *Chromatographia* **1987**, *24*, 701–704. [[CrossRef](#)]
28. Kim, Y.; Ahn, S.; Chang, T. Martin's Rule for High-Performance Liquid Chromatography Retention of Polystyrene Oligomers. *Anal. Chem.* **2009**, *81*, 5902–5909. [[CrossRef](#)]
29. Chester, T.L.; Coym, J.W. Effect of phase ratio on van't Hoff analysis in reversed-phase liquid chromatography, and phase-ratio-independent estimation of transfer enthalpy. *J. Chromatogr. A* **2003**, *1003*, 101–111. [[CrossRef](#)]
30. Thompson, J.F.; Honda, S.I.; Hunt, G.E.; Krupka, R.M.; Morris, C.J.; Powell, L.E.; Silberstein, O.O.; Towers, G.H.N.; Zacharius, R.M. Partition Chromatography and Its Use in the Plant Sciences. *Bot. Rev.* **1959**, *25*, 1–263. [[CrossRef](#)]
31. Skvortsov, A.; Trathnigg, B. Martin's rule revisited: Its molecular sense and limitations. *J. Chromatogr. A* **2003**, *1015*, 31–42. [[CrossRef](#)]
32. Tomlinson, E.; Poppe, H.; Kraak, J. Thermodynamics of functional groups in reversed-phase high performance liquid-solid chromatography. *Int. J. Pharm.* **1981**, *7*, 225–243. [[CrossRef](#)]
33. Golshan-Shirazi, S.; Guiochon, G. Modeling of preparative liquid chromatography. *J. Chromatogr. A* **1994**, *658*, 149–171. [[CrossRef](#)]
34. Kalbfuss, B.; Flockerzi, D.; Seidel-Morgenstern, A.; Reichl, U. Size-exclusion chromatography as a linear transfer system: Purification of human influenza virus as an example. *J. Chromatogr. B* **2008**, *873*, 102–112. [[CrossRef](#)] [[PubMed](#)]
35. Nguyen, H.S.; Kaspereit, M.; Sainio, T. Intermittent recycle-integrated reactor-separator for production of well-defined non-digestible oligosaccharides from oat β -glucan. *Chem. Eng. J.* **2021**, *410*, 128352. [[CrossRef](#)]
36. Villermaux, J. Chemical engineering approach to dynamic modelling of linear chromatography: A flexible method for representing complex phenomena from simple concepts. *J. Chromatogr. A* **1987**, *406*, 11–26. [[CrossRef](#)]

37. Nicoud, R.M. *Chromatographic Processes: Modeling, Simulation, and Design*; Cambridge Series in Chemical Engineering; Cambridge University Press: Cambridge, UK, 2015. [[CrossRef](#)]
38. Levenspiel, O. *Chemical Reaction Engineering*, 3rd ed.; John Wiley & Sons: Hoboken, NJ, USA, 1999.
39. Villermaux, J. Deformation of Chromatographic Peaks Under the Influence of Mass Transfer Phenomena. *J. Chromatogr. Sci.* **1974**, *12*, 822–831. [[CrossRef](#)]
40. Martin, A.J.P.; Synge, R.L.M. A new form of chromatogram employing two liquid phases. *Biochem. J.* **1941**, *35*, 1358–1368. [[CrossRef](#)]
41. Smit, H.C.; Smit, J.C.; de Jager, E.M. The role of the theoretical plate concept and gamma density functions in studies on mass transport and mass loadability of chromatographic columns. *Chromatographia* **1986**, *22*, 123–131. [[CrossRef](#)]
42. Spitzer, M.; Sabadini, E.; Loh, W. Entropically driven partitioning of ethylene oxide oligomers and polymers in aqueous/organic biphasic systems. *J. Phys. Chem. B* **2002**, *106*, 12448–12452. [[CrossRef](#)]
43. Rafferty, J.L.; Siepmann, J.I.; Schure, M.R. A molecular simulation study of the effects of stationary phase and solute chain length in reversed-phase liquid chromatography. *J. Chromatogr. A* **2012**, *1223*, 24–34. [[CrossRef](#)]
44. Lindsey, R.K.; Rafferty, J.L.; Eggimann, B.L.; Siepmann, J.I.; Schure, M.R. Molecular simulation studies of reversed-phase liquid chromatography. *J. Chromatogr. A* **2013**, *1287*, 60–82. [[CrossRef](#)] [[PubMed](#)]
45. Foley, J.P. Resolution equations for column chromatography. *Analyst* **1991**, *116*, 1275–1279. [[CrossRef](#)]
46. Bombaugh, K.J.; Levangie, R.F. High Resolution Gel Permeation Chromatography-Using Recycle. *Sep. Sci.* **1970**, *5*, 751–763. [[CrossRef](#)]
47. Seidel-Morgenstern, A.; Guiochon, G. Theoretical Study of Recycling in Preparative Chromatography. *AIChE J.* **1993**, *39*, 809–819. [[CrossRef](#)]
48. Bailly, M.; Tondeur, D. Recycle optimization in non-linear productive chromatography—I Mixing recycle with fresh feed. *Chem. Eng. Sci.* **1982**, *37*, 1199–1212. [[CrossRef](#)]
49. Grill, C.M. Closed-loop recycling with periodic intra-profile injection: A new binary preparative chromatographic technique. *J. Chromatogr. A* **1998**, *796*, 101–113. [[CrossRef](#)]
50. Kaspereit, M.; Sainio, T. Simplified Design of Steady-State Recycling Chromatography Under Ideal and Nonideal Conditions. *Chem. Eng. Sci.* **2011**, *66*, 5428–5438. [[CrossRef](#)]
51. Lochmüller, C.H.; Jiang, C.; Liu, Q.; Antonucci, V.; Elomaa, M. High-Performance Liquid Chromatography of Polymers: Retention Mechanisms and Recent Advances. *Crit. Rev. Anal. Chem.* **1996**, *26*, 29–59. [[CrossRef](#)]